Supplement of The Cryosphere, 14, 1475–1496, 2020
https://doi.org/10.5194/tc-14-1475-2020-supplement

The Cryosphere
Open Access

Supplement of

Quantification of seasonal and diurnal dynamics of subglacial channels using seismic observations on an Alpine glacier

Ugo Nanni et al.

Correspondence to: Ugo Nanni (ugo.nanni@univ-grenoble-alpes.fr)

Contents

S1 Seismic power methodology

S1.1 Temporal reconstruction

We show in Fig. S1 the seismic stations used to reconstruct the 'virtual station' seismic power . The overlapping period of mid-October 2017 is used to adjust, over a 10 days time window, the GDA seismic power to the ARG.B01 seismic power. The overlapping period of mid-June 2018 is used to adjust, over a 9 days time window, the ARG.B02 seismic power to the ARG.B01 seismic power.

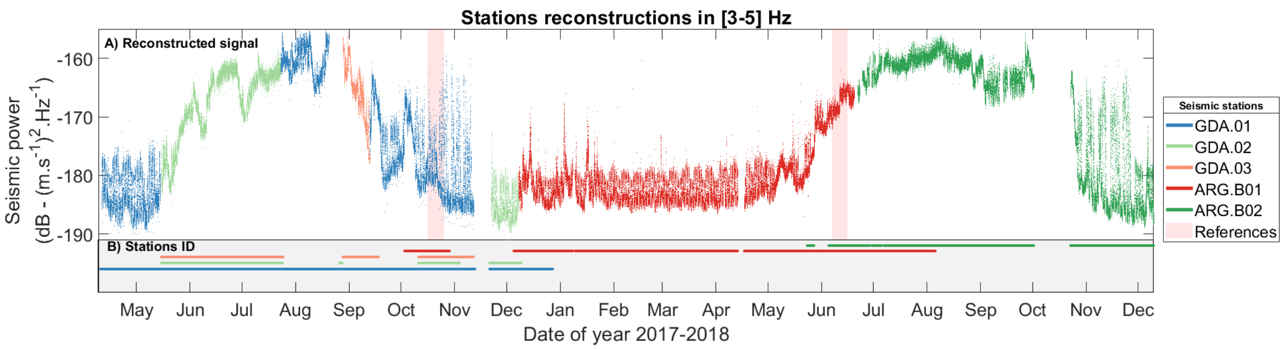

Figure S1. Time series of the corrected and assembled seismic power within the [3-5] Hz frequency range. We used this range to assemble the five stations seismic signals and apply the baseline shifts. Color coding refers to the corresponding stations and stations period of activity are shown in the light grey horizontal band. Light red vertical bands show the period used to constrain the baseline shift.

S1.2 Evaluating instrumental bias in δt interpretation

The subglacial channel-flow-induced seismic power P_w comparison between the different stations of our seismic network (Fig. 2) is shown in Fig. S2. We do not observe a significant time lag (< 5 min) between P_w measured at 2 stations 200 m appart (GDA.02 and GDA.03). It is important to note that this lag time δt_{inst} does not directly correspond neither to the water transit time, nor to the water flow speed between our instruments. This effect is mainly related to the seismic waves properties when propagating within the glacier. Our analyses is important for the intra-diurnal time scale, because this means that if Q and P_w are out of phase by more than δt_{inst} = 15 min (because Q measurement is done 600 m away from the seismic station) then this delay expresses subglacial hydraulic properties.

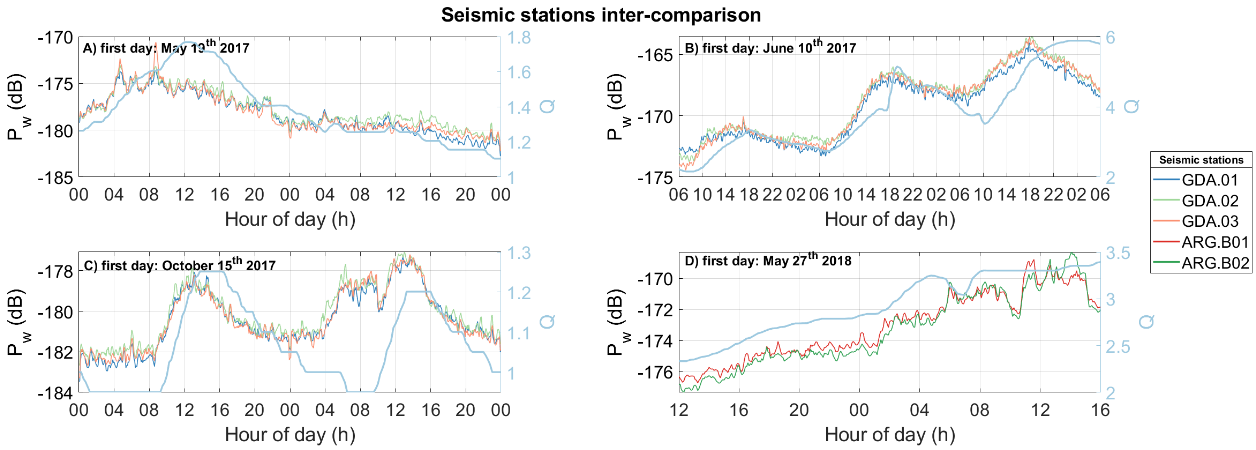

Figure S2. Time series of the measured seismic power within [3-7] hz at the different stations. (a) and(b) for the GDA network and (c) and (d) for the ARG network. Measurement is smoothed over 15 minutes, with one point every 15 minutes.

S1.3 Evaluating the potential bias from impulsive events contribution to seismic power

Over alpine glacier, impulsive events can be of diverse origins from serac falls (Roux et al., 2008), crevasses opening (e.g. Neave and Savage, 1970; Lindner et al., 2019), hydraulic fracturation, microseismicity linked with water discharge (Iken and Bindschadler, 1986; Preiswerk and Walter, 2018) or even basal stick-slip events as recently shown on Glacier d'Argentière by (Helmstetter et al., 2015). It is crucial to limit the influence of such impulsive events when aiming to study the subglacial channel-flow-induced seismic power. With respect to water tremor, impulsive events are characterized by short time-scale amplitude burst above the noise level by up to several order of magnitude. An important parameter for the Welch method is the time period dt over which we compute the Fourier transform FT. The seismic power P is calculated as $P= 10 \times log10\left[\left(\frac{FT}{dt}\right)^2\right]$. The longer dt, the greater number of impulsive events have the chance to occur. And the more the impulsive events within dt, the more they influence P and hidden the turbulent water flow source. The size of this window is limited by the frequencies investigated. To limit the impulsive events influence and still be able to investigate a frequency range down to 1 Hz we have chosen for our study a dt = 2 sec.

S1.4 Evaluating the anthropogenic signature influence on sub-diurnal timescales

Because the anthropogenic noise power presents a well-marked diurnal variability that could bias the analyses of the P_w analyses, we determine, from visual inspection in Fig. S3, the period during which P_w dominates the seismic power as averaged within [3-7] Hz frequency range. In Fig. S4 we show how a 5 day-lowpass filter allows us to study the mutliday variations of the seismic power while limiting the influence of the daily variations in the anthropogenic influence. We filter P_w to increase the influence of the multiday variability with respect to the short term variability.

S1.5 Evaluating the spatial sensitivity of the seismic record

During their journey from the source to the seismic station, seismic waves are attenuated. This behavior is related to energy dissipation within the propagation medium, here the ice, and because the higher the source to station distance, the larger the traveling distance and the thus lower the signal energy is. The attenuation of a signal with an amplitude of P_0 is defined a:

$$P_d = P_0 \frac{1}{d^n} e^{-\frac{2\pi df}{v_c Q}}, \tag{S1}$$

with d the distance from the source, n the geometrical exponent with n=*1* for surface waves and n=*2* for body waves, f the considered frequency, v_c the waves propagation velocity and Q the quality factor. The higher Q the more dissipative the medium is. Numerous values of Q have been proposed for alpine glacier ice within our frequency range, from Q=6±1 when considering only the uppermost glacier ice (first meters, Gusmeroli et al., 2010) up to Q=70 for the 100 to 500 m layer (Kohnen, 1969). For our investigation we cover Q = [5, 20, 60, 100]. We seek here to quantify the area around our seismic stations that can contribute within a certain energy, here 10 dB, to the measured seismic power P. We investigate two cases

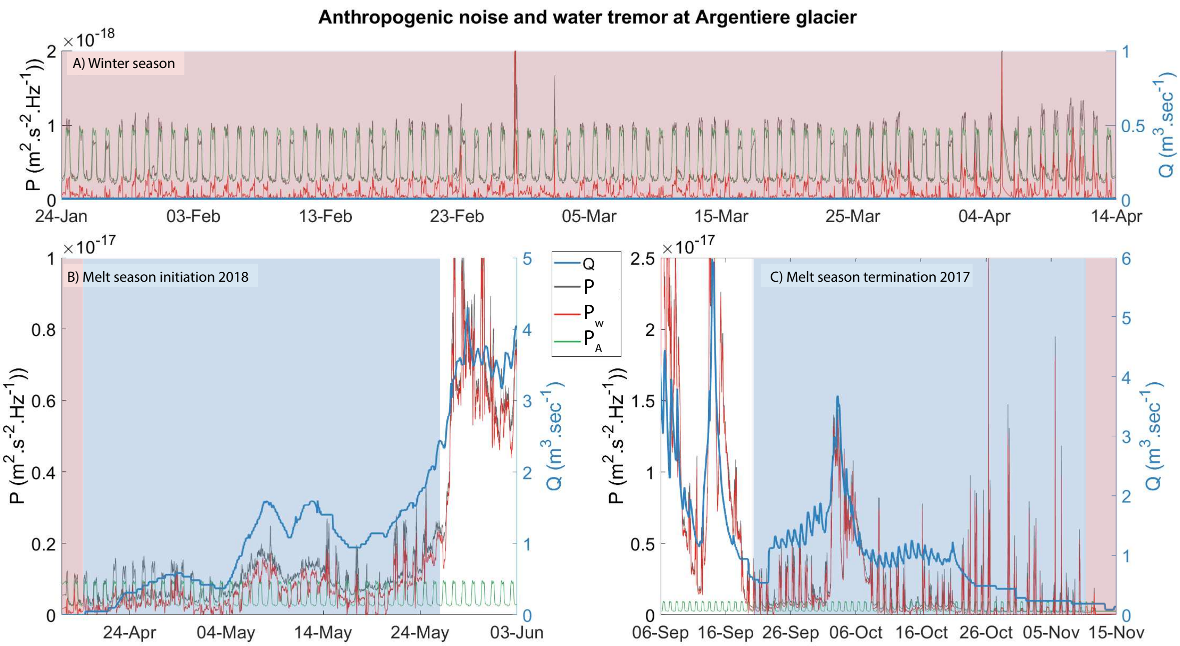

Figure S3. Time series of the measured seismic power (P, grey line), the daily-fitted anthropogenic noise seismic power (P_A, green line), the computed water tremor($P_w = P - P_A$, red line) and the measured water discharge (Q, blue line). The three periods (a) winter season, b) melt season initiation and c) melt season termination) presented are key to characterize the relative contributions of P_A and P_w to P. Shaded blue area represents the hydrological winter period where $Q<Q_{lim}$, light shaded blue area represents the period where the diurnal anthropogenic spectral is too pronounced to study P_w on a daily basis. x and y axis scale are not correspondant between the panels.

with a closest source S_1 located at d_1 = 1 and $d_{1'}$ = 200 m from the sensor. The former would represent a surface source, the latter a basal one at the glacier basis. We then searched for the distance $d(S_1,S_2)$ between the closest source S_1 and a second one S_2 where $P_{S_1,} - P_{S_2,}$=10 dB. This threshold value represent a relative value of 10% with respect to energy emitted from S_1 with no consideration of the absolute energy.

Figure S5 (a) shows that with respect to a surface source S_1 located at 1 m from the sensor, only the sources within a 10 m radius area will contribute to the [3-7] Hz signal energy by 10 dB, 10%, with respect to S_1. This area is reduced for increasing frequencies and quality factor. When we consider a source located at the glacier basis (Fig. S5 (b)), we observe that all sources within 500 to 1500 m from the sensor would contribute to the [3-7] Hz signal energy by 10%. The frequency and the quality factor effect is now dominated by the exponential decrease from equation S5. These results shows that if we consider water tremor signal within [3-7] Hz, a quality factor of Q=20, and a closest source at the glacier base then the measured signal will be dominated by sources located within a radius of 800 m from our sensor.

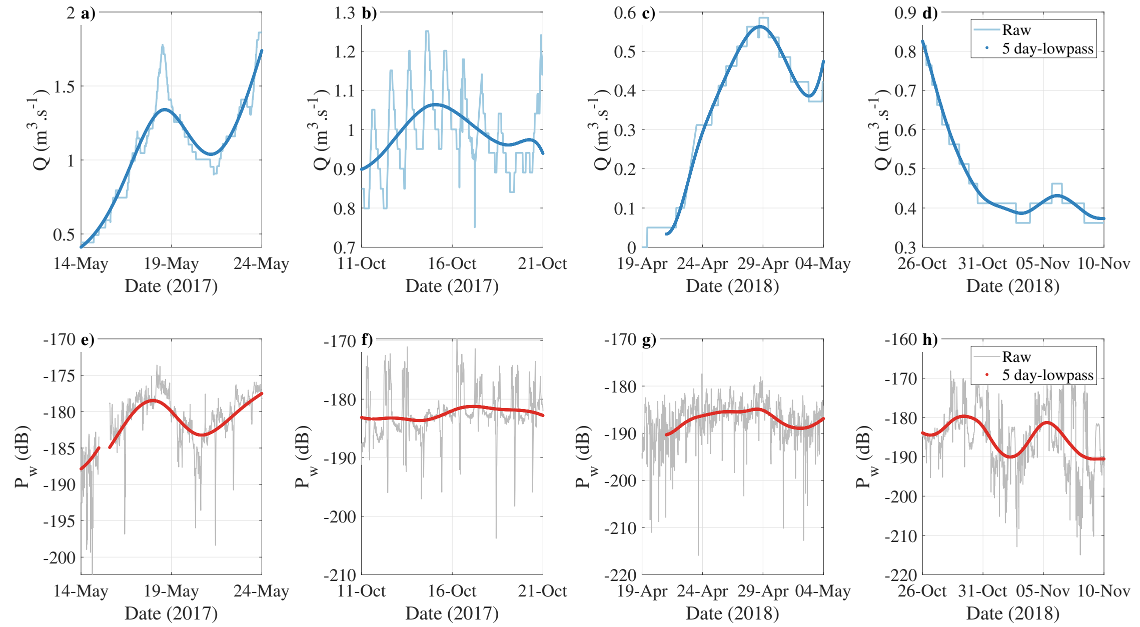

Figure S4. (a) to (d) Time series of the measured water discharge Q at a 15 min time step (shaded blue line) and the 5 day-lowpass filtered Q (dark blue line) for the tips of both 2017 and 2018 melt seasons. (e) to (h) Time series of the subglacial induced seismic power P_w at a 15 min time step (shaded grey line) and the 5 day-lowpass filtered Q (dark red line) for the tips of both 2017 and 2018 melt seasons.

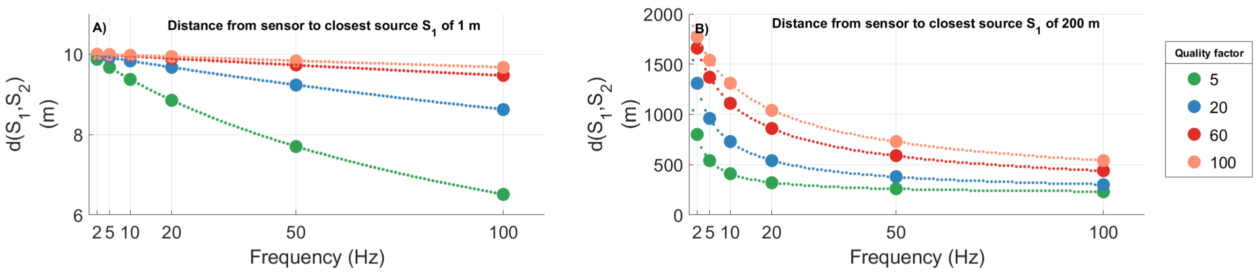

Figure S5. Synthetic effect of attenuation on seismic surface wave (n=1). The two panels show the distance $d(S_1, S_2)$ of a source S_2 to the closest source S_1 where the attenuation is such that $P(S_1)_{sensor} = (S_2)_{sensor} + 10$ dB depending on the frequency and the quality factor. This distance represents the radius of source location within which any given source will contribute for at least 10% to the recorded seismic power with respect to a source located at distance of 1 m (left panel) and 200 m (right panel) from the sensor.

S2 Theoretical channel properties

S2.1 Evaluating theoretical channels dynamics with Röthlisberger (1972)' equations

In his paper, Röthlisberger (1972) proposes the two following equations for steady-state channels at equilibrium:

$$4R^2 = \left(\frac{2^{4/3}\rho_w g}{\pi^2}\right)^{3/8} k^{-3/4} Q^{3/4} \left(\frac{dp}{dx}\right)^{-3/8} \tag{S2}$$

$$\frac{dp}{dx} = Bk^{-6/11}(nA^{-8n/11}Q^{-2/11}(P-p)^{8n/11}), \tag{S3}$$

with $\frac{dp}{dx}$ the hydraulic pressure gradient S, P the cryostatic pressure, k the channel roughness, B equals to constant, A and n ice flow parameters. Taking equation S3 and considering constant effective pressure (P-p) and flow parameters leads to

$S \propto Q^{-2/11}$.

Now inserting equation S3 in S2 and considering constant channel roughness, leads to

$$R^2 \propto Q^{3/4}\left(Q^{-2/11}\right)^{-3/8},$$
$$R^2 \propto Q^{66/88}Q^{6/88},$$
$$R^2 \propto Q^{9/11},$$
$$R \propto Q^{9/22}.$$

For a steady-state channel not in equilibrium with Q that responds solely through changes in S this leads to

$$S^{3/8} \propto Q^{3/4},$$
$$S^{3/8} \propto Q^{6/8},$$
$$S \propto Q^2.$$

S2.2 Evaluating theoretical melt and creep rates with Hooke (1984)' equations

We use here equations 6 and 8 of Hooke (1984) to evaluate the theoretical melt rate $\dot{m}$ and creep rate $\dot{r}$, which are as follows

$$\dot{m} = C_2 Q^{3/5} sin(\beta)^{6/5}, \tag{S4}$$
$$\dot{r} = C_3 \frac{Q^{2/5}}{sin(\beta)^{1/5}} H^3, \tag{S5}$$

with H the ice thickness, β the surface slope, C_2 and C_3 constant. We use the values of Hooke (1984) for the two constants: $C_2 = 3.731e^{-5}$ m$^{-4/5}$ s$^{-2/3}$ and $C_2 = 5.71e^{-14}$ m$^{-16/5}$ s$^{-3/5}$. We show in Fig. S6 the theoretical channel growth rate for a R-channel at steady state. Calculations are made following Eqs.(S5) and (S4). The equilibrium condition, melt rate equals creep rate, is verified when the channel growth rate equals zero. This shows that for a given glacier geometry (slope an thickness), the equilibrium condition depends only on the water discharge. The more the channel number, the less the discharge per channel for a given output discharge and therefore the longer the equilibrium condition can be satisfied.

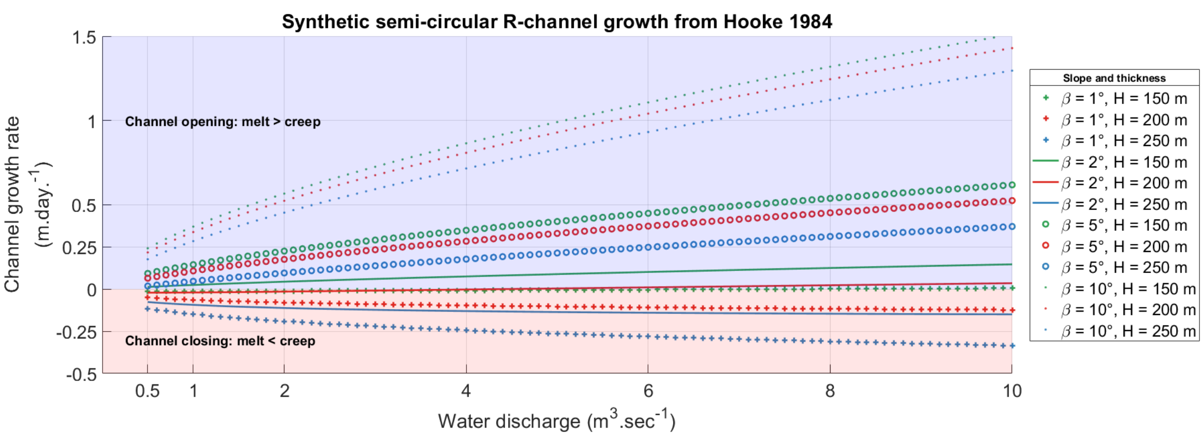

Figure S6. Synthetic evolution of a semi-circular shaped R-channel. Melt ($\dot{m}$) and creep ($\dot{r}$) rate are calculated from Eqs.(S5) and (S4) of Hooke (1984) with the constants C_2 and C_3 as in Hooke (1984), the slope and the ice thickness are shown in the legend. The curves show $\dot{m}$ - $\dot{r}$, with the shaded blue area $\dot{m} > \dot{r}$ and the shaded red area $\dot{m} < \dot{r}$.

We show in Fig. S7 the synthetic closure rate of an open channel and compared it to the observed channel radius changes, assuming that the hydraulic radius changes equals the channel radius changes. Our comparison show that for the observed range of channel radius changes (5 to 10 $\%$) the channel response time is of about a couple of hours. Therefore channel could creep fast enough at sub-diurnal timescale to equilibrate channel growth by melt.

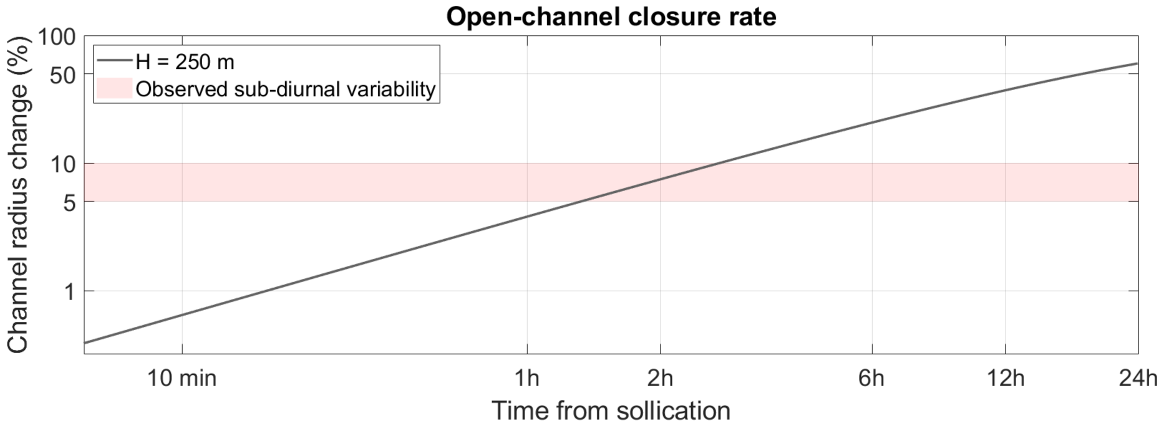

Figure S7. Synthetic closure rate of an open-channel computed for a channel size $R(t) = R_0 e^{(-c\sigma_i^n t)}$, with $R(t)$ the channel radius through time, R_0 the initial channel size, $c = 1e^{-24}$ Pa^{-3}.s^{-1} the ice viscosity (Cuffey and Paterson, 2010), $n = 3$ the Glen's flow constant (Cuffey and Paterson, 2010) and $\sigma = \rho_i g h_i$ with ρ_i = 900 kg.m^{-3} the ice density, $g = 9.81$ m.s^{-2} the acceleration due to gravity and $h = 250$ m the glacier thickness. The time is defined with $t = 0$ the moment when channel become open (free flow) and the change are expressed in $\%$ with respect to the initial size, 10% being $R(t) = R_0 \times 0.9$. Shaded red area shows the observed sub-diurnal variability in hydraulic radius at Glacier d'Argentière during summer of years 2017 and 2018.

We estimate melt and creep rates using equations 6 and 8 of Hooke (1984) as here above. From mid-May to early July, hydraulic radius R increases by a factor of 3 to 4. For constant number of channels, this results in summer channels radius of [1.00 - 1.25] m. Over the summer R varies by 4 to 8 $\%$ on a daily basis, which corresponds to diurnal changes of [4 - 10] cm.day^{-1} in channel radius. Such changes are on the same order of magnitude as those calculated with Hooke (1984) equations which predict a melt rate of about [10-25] cm.day^{-1} and creep rate of about [5-20] cm.day^{-1} for these periods ($Q \propto$ 5 m^3.sec^{-1}). This shows that subglacial channels have the capability to adjust their size on a daily basis in response to water input variability. Channels can thus rapidly close during the water discharge decrease and possibly keep a closed-flow behavior over summer. This supports the plausibility the channels' diurnal dynamic proposed previously based on our observations.

S3 Codes for seismic processing

We show here our two codes used to process the raw SAC seismic data.

Listings

S3.1 Remove instrumental response with SAC

```
#!/bin/bash
# ==========================================================
# ----------------------------------------------------------
path2dat=/media/ugonanni/2E3D-8697/DATA/ARGENTIERE/ARG_Borehole_Ugo
path2sac=$path2dat/SACt
path2sacday=$path2sac/DAY
path2saccorr=$path2sac/Corr
# ----------------------------------------------------------
cd $path2sacday
 ls A*.SAC > sac_list # list of all data

for file in `cat sac_list`;do
    new_file=`echo $file | sed -e 's#DAY.SAC#DAY_Corr.SAC#g' `
    echo $new_file
    echo $file

sac <<EOF
setbb pzfile "./PZ.ARG.B01.normgain3_A0625" # PZ files for corrections
r $file
rmean
rtr
taper w 0.00001
trans from polezero S %pzfile to vel freqlim 0.25 0.5 450 490
w $new_file
quit
EOF
mv $new_file $path2saccorr/.
done
```

Listing 1. Code to correct SAC files from instrumental response

S3.2 Compute PSD with Python

```
#!/usr/bin/env python3
@author: ugonanni

# ----------------------------------------------------------
# Import packages
# ----------------------------------------------------------

import glob
import matplotlib.pyplot as plt
import numpy as np
import obspy
from os.path import join
from obspy.core import read
from obspy.core import UTCDateTime

```

```python
from scipy.signal import welch, hanning
from scipy import signal

import os

import scipy
import scipy.fftpack

from scipy import pi
from scipy.fftpack import fft

import time

import astropy.time
import dateutil.parser

import datetime
import pandas as pd
# ----------------------------------------------------------------------
# Define path
# ----------------------------------------------------------------------

path2dat = '/media/ugonanni/Nanni/DATA_ARG_backup/GDA/SAC/RAW'
path2sav = '/home/ugonanni/Share/PhD/DATA/PWelch_output'


filename = ''

# ----------------------------------------------------------------------
# Define parameters
# ----------------------------------------------------------------------


# Pwelch parameters
l_win = 4 # secondes
# window
window = 'hanning'
# detrend
detrend = 'False'
# Number of segments
nb_seg = 2**19
lseg = l_win/2


# Initialize PSD vector
len_PSD = 1001


# min and max frequency to select frequency bands
fmin = [1,5,10,20]
fmax = [5,10,20,50]

# define time according to first day of 2017, i.e. DOY 2017
time17 = astropy.time.Time(datetime.datetime(2017, 1, 1, 0, 0))

t17 = time17.jd-1

# ----------------------------------------------------------------------
# Compute PWelch
```

```
# -----------------------------------------------------------------------------

it_day = 0
# select file type

for ext in ['*03..1Z*']:

    nbfiles = len(glob.glob(path2dat + '/' + ext))
    for file in sorted(glob.glob(path2dat + '/'+ ext)):

        # read data and time
        data = read(file)
        Time_data = data[0]


        # define names
        t = Time_data.stats.starttime
        name = '' + Time_data.stats.network + '.' + Time_data.stats.station + '.'  + Time_data.stats.channel + '.' + str(t.year) + '.' + str(t.month) + '.' + str(t.day)
        print(name)


        # File duration in secondes
        duration = Time_data.stats.endtime - Time_data.stats.starttime

        # Sampling frequency of the time series.
        fs = int(np.round(Time_data.stats.sampling_rate))

        # number of points of the data
        nb_psd = duration/l_win

         # define PSD matrix
        PSD_matrix = np.empty([int(nb_psd),int(len_PSD)])
        Time_vector = []
        Hydro = np.empty([int(nb_psd),len(fmin)])
        Hydro_std = np.empty([int(nb_psd),len(fmin)])

        # compute PSD
        for jj in range(0,int(nb_psd)):
            # extract short time
            tmp = Time_data[jj*l_win*fs:(jj+1)*l_win*fs]
            nb_points = len(tmp)

            # Length of each segment.
            nperseg = fs*lseg # here 1 secondes

            # Number of points to overlap between segments.
            noverlap = nperseg / 2

            # Time associated with Pwelch is centered on the window
            a = int(((jj*l_win))+(l_win/2))

            Time_vector.append(Time_data.stats.starttime + a)


            # Compute PSD with welch
            if nb_points >= nperseg:
                f, Pxx = welch(tmp, fs, window=window, nperseg=nperseg, noverlap=noverlap, detrend=False, return_onesided=True)
```

```
                PSD_matrix[jj,:] = Pxx


        Time_vector = np.asarray(Time_vector)

        Tdoy = np.empty(len(Time_vector))
        for jj in range(0,len(Time_vector)):
            tim = astropy.time.Time(datetime.datetime(Time_vector[jj].year, Time_vector[jj].month, Time_vector[jj].day, Time_vector[jj].hour, Time_vector[jj].minute, Time_vector[jj].second))
            Tdoy[jj] =  tim.jd
        Tdoy = Tdoy - t17
        #plt.plot(Time_data)
        #plt.show()


        print(str(it_day+1) + ' over '  + str(nbfiles))
        it_day = it_day + 1
        # save data
        try:
            np.savetxt(path2sav + '/' + name + '_PSD_Tcorr_'  + str(l_win) +'sec',PSD_matrix)
            np.savetxt(path2sav + '/' + name + '_Time_Tcorr_' + str(l_win) +'sec',Tdoy)
        except IOError:
            print("Not enough space")
            os.system('pause')
             # We try again
            try:
                np.savetxt(path2sav + '/' + name + '_PSD_Tcorr_'  + str(l_win) +'sec',PSD_matrix)
                np.savetxt(path2sav + '/' + name + '_Time_Tcorr_' + str(l_win) +'sec',Tdoy)
            except IOError:
                print("Still not enough space")





    np.savetxt(path2sav + '/'+ name  + '_Frequency_Tcorr_' + str(l_win) +'sec',f)

    # loop on each days for concatenating
```
Listing 2. Code to compute PSD from 1 day SAC files

References

Cuffey, K. M. and Paterson, W. S. B.: The physics of glaciers, Academic Press, 2010.

Gusmeroli, A., Clark, R. A., Murray, T., Booth, A. D., Kulessa, B., and Barrett, B. E.: Seismic wave attenuation in the uppermost glacier ice of Storglaciären, Sweden, Journal of Glaciology, 56, 249–256, 2010.

Helmstetter, A., Nicolas, B., Comon, P., and Gay, M.: Basal icequakes recorded beneath an Alpine glacier (Glacier d'Argentière, Mont Blanc, France): Evidence for stick-slip motion?, Journal of Geophysical Research: Earth Surface, 120, 379–401, 2015.

Hooke, R. L.: On the role of mechanical energy in maintaining subglacial water conduits at atmospheric pressure, Journal of Glaciology, 30, 180–187, 1984.

Iken, A. and Bindschadler, R. A.: Combined measurements of subglacial water pressure and surface velocity of Findelengletscher, Switzerland: conclusions about drainage system and sliding mechanism, Journal of Glaciology, 32, 101–119, 1986.

Kohnen, H.: Über die Absorption elastischer longitudinaler Wellen im Eis, Polarforschung, 39, 269–275, 1969.

Lindner, F., Laske, G., Walter, F., and Doran, A. K.: Crevasse-induced Rayleigh-wave azimuthal anisotropy on Glacier de la Plaine Morte, Switzerland, Annals of Glaciology, 60, 96–111, 2019.

Neave, K. and Savage, J.: Icequakes on the Athabasca glacier, Journal of Geophysical Research, 75, 1351–1362, 1970.

Preiswerk, L. E. and Walter, F.: High-Frequency (> 2 Hz) Ambient Seismic Noise on High-Melt Glaciers: Green's Function Estimation and Source Characterization, Journal of Geophysical Research: Earth Surface, 123, 1667–1681, 2018.

Röthlisberger, H.: Water pressure in intra-and subglacial channels, Journal of Glaciology, 11, 177–203, 1972.

Roux, P.-F., Marsan, D., Métaxian, J.-P., O'Brien, G., and Moreau, L.: Microseismic activity within a serac zone in an alpine glacier (Glacier d'Argentiere, Mont Blanc, France), Journal of Glaciology, 54, 157–168, 2008.